JOURNAL OF GEOPHYSICAL RESEARCH, VOL. 106, NO. C8, PAGES 16,997–17,011, AUGUST 15, 2001

Frontshear and backshear instabilities of the mean longshore current

Asunción Baquerizo,[1] Miquel Caballeria,[2] Miguel A. Losada,[1] and Albert Falqués[3]

Abstract. An analytical model based on *Bowen and Holman* [1989] is used to prove the existence of instabilities due to the presence of a second extremum of the background vorticity at the front side of the longshore current. The growth rate of the so-called frontshear waves depends primarily upon the frontshear but also upon the backshear and the maximum and the width of the current. Depending on the values of these parameters, either the frontshear or the backshear instabilities may dominate. Both types of waves have a cross-shore extension of the order of the width of the current, but the frontshear modes are localized closer to the coast than are the backshear modes. Moreover, under certain conditions both unstable waves have similar growth rates with close wave numbers and angular frequencies, leading to the possibility of having modulated shear waves in the alongshore direction. Numerical analysis performed on realistic current profiles confirm the behavior anticipated by the analytical model. The theory has been applied to a current profile fitted to data measured during the 1980 Nearshore Sediment Transport Studies experiment at Leadbetter Beach that has an extremum of background vorticity at the front side of the current. In this case and in agreement with field observations, the model predicts instability, whereas the theory based only on backshear instability failed to do so.

1. Introduction

In general, the wave-driven mean longshore current in the surf zone has a horizontal profile that increases seaward of the shoreline, reaches a maximum, and then decreases to a vanishing value beyond the breaking line. Thus the background vorticity (V_x/ζ, where V_x is the horizontal shear of the current and ζ is the total mean depth) has at least one extremum seaward of the peak of the current. This is a necessary condition (Rayleigh condition) for the current to be unstable with respect to alongshore traveling perturbations so-called shear waves. *Bowen and Holman* [1989] (hereinafter referred to as BH) illustrated the mechanism of the shear instability by means of a simple velocity profile with only one local extremum of the background vorticity on the seaward side of the current. In this case, the instability was clearly related to the extremum of the background vorticity at the back (seaward side of the current), and their model showed a good agreement with the field observations of *Oltman-Shay et al.* [1989]. Following BH, most of the theoretical analysis on linear shear waves have considered current profiles with only one seaward extremum of the background vorticity and thus have been related to the backshear [see, e.g., *Putrevu and Svendsen*, 1992; *Dodd and Thornton*, 1990; *Falqués and Iranzo*, 1994; *Caballeria et al.*, 1998]. Laboratory experiments by *Reniers et al.* [1997] have also shown good agreement between measured and predicted wavenumbers and frequencies of shear waves on the basis of the backshear instability.

Dodd et al. [1992], comparing stability properties at a flat and at a barred beach, observed that for the latter more than one unstable mode may arise. Since the background vorticity of the current in this case had more than one extremum, they associated one of them to the backshear and the other to the frontshear. They claimed that the mode associated to the frontshear over the bar was the fastest growing mode, while the second fastest one was the mode related to the backshear. They therefore concluded that for barred beaches the backshear may not be so important. Also, some studies on nonlinear shear waves [see, e.g., *Allen et al.*, 1996; *Ozkan-Haller and Kirby*, 1999] have considered profiles of the basic steady current with two inflexion points, although the nonlinear analysis was based on the linearly dominant mode without caring about its origin. Those studies and the present paper suggest that under some circumstances the low-frequency modulation of the shear waves could be due to the interference of the frontshear and the backshear modes.

In this paper, the existence and the properties of two instability modes, one related to the extremum of the background vorticity seaward of the peak of the current (and to the backshear (BS) mode) and the other related to the extremum shoreward of the peak of the current (and to the frontshear (FS) mode) are investigated in detail. To this end a velocity profile with a maximum and two inflexion points at both sides of it is analyzed. The characteristics, wavelength, frequency, flow pattern, and conditions under which one or both modes are dominant are investigated. In order to deal with a simple analytical solution, following BH, an idealized current profile on a horizontal bottom is considered. Next, a similar analysis on realistic current and topography profiles, carried out by means of numerical simulation including bottom friction and turbulent momentum diffusion, confirms the validity of the idealized theoretical results. It is shown that under certain

[1]Grupo de Puertos y Costas, Universidad de Granada, Granada, Spain.
[2]Departament de Física y Matemàtica Aplicades, Universitat de Vic Carrer de la Laura, Vic, Spain.
[3]Departament de Física Aplicada, Universitat Politècnica de Catalunya Jordi Girona, Barcelona, Spain.

Paper number 2001JC900004.
0148-0227/01/2001JC900004$09.00

conditions the frontshear is indeed dominant. Moreover, there are longshore current profiles that have frontshear and backshear waves of similar growth rates, making plausible the occurrence of a field modulated in the longitudinal direction. Finally, instability analysis of a velocity profile obtained from data measured at Leadbetter Beach [*Thornton and Guza*, 1986] that shows an inflexion point at the front side is performed. Results are compared with field data observations, showing good agreement with measured frequency-cyclic wave number spectra.

The paper is organized as follows. The theoretical framework is presented in section 2. The simple analytical model is developed in section 3. The numerical simulation for realistic conditions, including the comparison with Leadbetter Beach field data observations, is described in section 4. The conclusions are given in section 5.

2. Formulation

The shallow water equations for momentum and mass conservation are considered as governing equations:

$$\frac{\partial v_i}{\partial t} + \sum_{j=1}^{2} v_j \frac{\partial v_i}{\partial x_j} + g \frac{\partial \eta}{\partial x_i} = \frac{1}{\rho \zeta} (\tau_{ri} + \tau_{bi} + \tau_{ui}), \qquad (1)$$

$$i = 1, 2,$$

$$\frac{\partial \eta}{\partial t} + \sum_{j=1}^{2} \frac{\partial}{\partial x_j} (\zeta v_j) = 0. \qquad (2)$$

The coordinate system is taken with the x_3 axis pointing vertically upward. The free surface for still water corresponds to $x_3 = 0$. The x_2 axis is at the still water shoreline, and x_1 is oriented pointing offshore. The bottom profile is given by $x_3 = -h(x_1)$, and the free surface elevation is given by $x_3 = \eta(x_1, x_2, t)$. The total depth is $\zeta = h + \eta$, ρ stands for the water density, t stands for time, and $\mathbf{v}$ stands for the depth-averaged horizontal velocity. The wind/swell wave forcing is given by $\boldsymbol{\tau}_r$, and dissipation comes from bottom friction, $\boldsymbol{\tau}_b$, and turbulent lateral momentum diffusion $\boldsymbol{\tau}_v$. The wave term is calculated from the radiation stress tensor S_{ij} as

$$\tau_{ri} = -\frac{\partial S_{ij}}{\partial x_j}, \qquad i = 1, 2. \qquad (3)$$

The bottom shear stress is given by

$$\boldsymbol{\tau}_b = -c_d \rho \langle |\mathbf{u}_0 + \mathbf{v}| (\mathbf{u}_0 + \mathbf{v}) \rangle, \qquad (4)$$

where $\mathbf{u}_0$ is orbital velocity, c_d is the drag coefficient for bottom friction, and brackets $\langle\ \rangle$ mean temporal average in the incoming short wave period. The turbulent lateral momentum diffusion is evaluated through

$$\tau_{ui} = \frac{\partial}{\partial x_j} \left[\rho \nu_t \zeta \left(\frac{\partial v_j}{\partial x_i} + \frac{\partial v_i}{\partial x_j} \right) \right], \qquad i = 1, 2, \qquad (5)$$

where ν_t is the kinematic eddy viscosity.

The basic undisturbed state consists of a longshore current,

$$v_1 = 0 \qquad v_2 = V(x_1), \qquad (6)$$

and a setup/setdown of the free surface,

$$\eta = \eta_0(x_1), \qquad (7)$$

which are a steady solution of (1) and (2). An effective depth is defined by

$$h_e = h + \eta_0, \qquad (8)$$

and the cross-shore coordinate x is shifted with respect to x_1 in order to have $x = 0$ at the effective shoreline (hereinafter it will take the coordinates x, $y = x_2$). Then the free surface elevation measured from the basic undisturbed state η_0 is

$$\xi(x, y, t) = \eta(x, y, t) - \eta_0(x), \qquad (9)$$

and the total depth is

$$\zeta = h + \eta_0 + \xi = h_e + \xi. \qquad (10)$$

To perform linear stability analysis, a small perturbation is superimposed to the basic steady flow and the free surface elevation:

$$v_1 = u(x, y, t) = \hat{u}(x) e^{i(ky - \sigma t)}, \qquad (11)$$

$$\begin{aligned} v_2 &= V(x) + v(x, y, t) = V(x) + \hat{v}(x) e^{i(ky - \sigma t)}, \\ \eta &= \eta_0(x) + \xi(x, y, t) = \eta_0(x) + \hat{\xi}(x) e^{i(ky - \sigma t)}, \end{aligned} \qquad (12)$$

where the real number k takes account of the alongshore periodicity of wavelength $\lambda_s = 2\pi/k$, the real part σ_r of σ gives the angular frequency of the shear wave, and its imaginary part σ_i gives the growth rate. The perturbation is periodic in time with period $T_s = 2\pi/\sigma_r$ and propagates in the longshore direction with celerity $c_r = \sigma_r/k$.

By using the weak-current approximation [*Dodd*, 1994], using a small angle of incidence, and taking orbital velocity amplitude

$$u_0 = \frac{\gamma}{2} \sqrt{g\zeta}, \qquad (13)$$

where γ is the breaking index, the bottom friction becomes

$$\begin{aligned} \tau_{bx} &= -\rho c_d \frac{2}{\pi} \gamma \sqrt{g\zeta}\, u \\ \tau_{by} &= -\rho c_d \frac{2}{\pi} \gamma \sqrt{g\zeta}\, (V + v). \end{aligned} \qquad (14)$$

By inserting (12) into the governing equations (1) and (2) upon linearization and taking (5) and (14) into account the system of three ordinary differential equations is obtained:

$$\begin{aligned} ik(V - c)\hat{u} = {} & -g\hat{\xi}_x - c_d \frac{2\gamma}{\pi} \sqrt{\frac{g}{h_e}}\, \hat{u} \\ & + \nu_t \left[2\hat{u}_{xx} + 2 \frac{\hat{u}_x h_{ex}}{h_e} - k^2 \hat{u} + ik \left(\hat{v}_x + \frac{V_x \hat{\xi}}{h_e} \right) \right] \\ & + \nu_{tx} 2\hat{u}_x, \end{aligned} \qquad (15)$$

$$\begin{aligned} V_x \hat{u} + ik(V - c)\hat{v} = {} & -ikg\hat{\xi} - c_d \frac{\gamma}{\pi} \sqrt{\frac{g}{h_e}} \left(\hat{v} - \frac{V}{2h_e} \hat{\xi} \right) \\ & + \nu_t \left[ik \left(\hat{u}_x + \frac{h_{ex}}{h_e} \hat{u} \right) + \hat{v}_{xx} + \frac{h_{ex}}{h_e} \hat{v}_x - 2k^2 \hat{v} + \frac{V_x}{h_e} \hat{\xi}_x \right. \\ & \left. + V_{xx} \frac{\hat{\xi}}{h_e} \right] + \nu_{tx} \left(ik\hat{u} + \hat{v}_x + \frac{V_x}{h_e} \hat{\xi} \right), \end{aligned} \qquad (16)$$

$$h_e \hat{u}_x + h_{ex} \hat{u} + ikh_e \hat{v} + ik(V - c)\hat{\xi} = 0, \qquad (17)$$

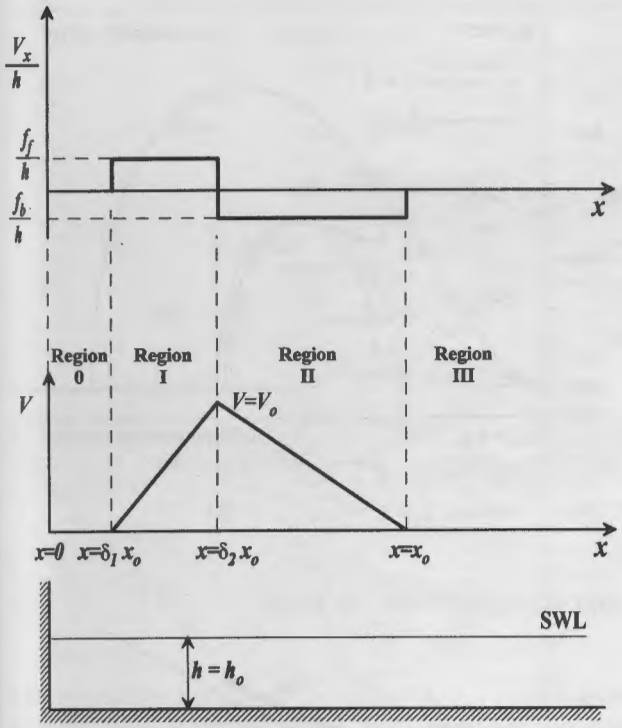

Figure 1. Definition sketch of the extended *Bowen and Holman* [1989] model.

which is an eigenproblem for the eigenvalue $c = \sigma/k$ and the eigenfunction $(\hat{u}, \hat{v}, \hat{\xi})$. Here any perturbation on the forcing due to the feedback from the instability into the incident wave field has been neglected. After discretization by spectral methods, the stability eigenproblem is solved by standard routines [*Falqués and Iranzo*, 1994] to obtain the dispersion lines (k, σ_r) and the instability curves (k, σ_i).

3. Extended *Bowen and Holman* [1989] Model

The existence of an instability due to an extremum of the background vorticity at the front side of the velocity profile and the way it coexists with the traditional backshear instability is investigated in this section. In order to have an analytical description a simple case based on BH is considered. An infinitely long flat-bottom beach of constant depth $h = h_0$, bounded by a vertical wall at $x = 0$, and a piecewise longitudinal current that consists of four regions are assumed (see Figure 1). In region 0, which extends from $x = 0$ to $x = \delta_1 x_0$ $(0 \le \delta_1 < 1, x_0 > 0)$, the velocity is zero. In region I the current increases linearly from $V = 0$ at $x = \delta_1 x_0$ to its maximum value $V = V_0$ at $x = \delta_2 x_0$ $(\delta_1 < \delta_2 < 1)$. In region II the velocity varies linearly from V_0 at $x = \delta_2 x_0$ to $V = 0$ at $x = x_0$. Finally, the velocity current is zero in region III, which extends seaward of $x = x_0$.

The corresponding background vorticity is a discontinuous function that is zero in regions 0 and III, has a positive constant value $V_x/h = f_f/h$ in region I, and has a negative constant value $V_x/h = f_b/h$ in region II. Notice that for $\delta_1 = 0$ the profile coincides with that analyzed by BH, with V_x/h having only one extremum in region II. For $\delta_1 > 0$, there is an additional extremum of the background vorticity in region I.

To seek an analytical solution, bottom friction and turbulent momentum diffusion are disregarded, and the rigid lid assumption is adopted, i.e., $d\eta/dt$ is negligible in comparison to horizontal fluxes. From this latter hypothesis and the mass conservation (17), a stream function representation of the flow follows:

$$hu(x, y, t) = -\Psi_y$$
$$hv(x, y, t) = \Psi_x \tag{18}$$

with

$$\Psi = \mathrm{Re}\,[\psi(x)e^{i(ky-\sigma t)}]. \tag{19}$$

Plugging (19) into (15) and (16) results in an expression for the free surface elevation

$$\xi(x) = -\frac{1}{gh}[(V - c)\psi_x - V_x\psi] \tag{20}$$

and a governing equation

$$(V - c)\left[\psi_{xx} - k^2\psi - \frac{\psi_x h_x}{h}\right] - h\psi\frac{\partial}{\partial x}\left(\frac{V_x}{h}\right) = 0. \tag{21}$$

Introducing dimensionless variables x', y', ξ', u', v', Ψ', and t' such that

$$x = x_0x', \quad y = x_0y', \quad \xi = h_0\xi', \quad h_e = h_0h_e',$$
$$t = \frac{x_0}{V_0}t', \quad u = V_0u', \quad v = V_0v', \tag{22}$$
$$V = V_0V', \quad c = V_0c', \quad \Psi = x_0h_0V_0\Psi',$$

the simple topography and velocity profile of the model (21) reduces to

$$\psi'_{xx} - k'^2\psi' = 0. \tag{23}$$

Henceforth the dimensionless variables will be noted without prime.

The boundary conditions $\psi(x = 0) = 0$ and $\psi(x = \infty) = 0$ are applied to (23) at the shoreline and far offshore. The solution to this boundary problem is

$$\begin{aligned}
&\text{Region 0 } \psi_0 = A_0 \sinh(kx)\\
&\text{Region I } \psi_1 = A_1 \sinh(kx) + B_1 \cosh(kx)\\
&\text{Region II } \psi_2 = A_2 \sinh(kx) + B_2 \cosh(kx)\\
&\text{Region III } \psi_3 = A_3e^{-kx}
\end{aligned} \tag{24}$$

To ensure the continuity of the stream function ψ and of the sea surface elevation ξ, the following matching conditions at the interfaces are imposed:

$$\begin{aligned}
&\psi_0(\delta_1) = \psi_1(\delta_1), \quad \psi_1(\delta_2) = \psi_2(\delta_2),\\
&\psi_2(1) = \psi_3(1), \quad \xi_0(\delta_1) = \xi_1(\delta_1),\\
&\xi_1(\delta_2) = \xi_2(\delta_2), \quad \xi_2(1) = \xi_3(1).
\end{aligned} \tag{25}$$

Conditions (25) constitute a linear system for the unknown coefficients A_0, A_1, B_1, A_2, B_2, and A_3. A nontrivial solution requires the corresponding matrix to be singular, i.e., a certain condition on σ. From (25) the following relations can be obtained:

$$\frac{A_0}{A_1} = 1 - \frac{c_1}{s_1}\frac{B_1}{A_1}, \tag{26}$$

$$\frac{B_1}{A_1} = \frac{f_f s_1^2}{\sigma - f_f s_1 c_1}, \tag{27}$$

$$(k - \sigma)\left[\frac{B_2}{A_2} - \frac{B_1}{A_1}\right] + (f_b - f_f)\left[s_2^2 + s_2 c_2\left(\frac{B_1}{A_1} + \frac{B_2}{A_2}\right) + c_2^2 \frac{B_1}{A_1}\frac{B_2}{A_2}\right] = 0, \tag{28}$$

$$\frac{B_2}{A_2} = -\frac{\sigma + e_0 s_0 f_b}{\sigma + e_0 c_0 f_b}, \tag{29}$$

where

$$s_1 = \sinh(\delta_1 k), \quad c_1 = \cosh(\delta_1 k),$$
$$s_2 = \sinh(\delta_2 k), \quad c_2 = \cosh(\delta_2 k), \tag{30}$$
$$s_0 = \sinh(k), \quad c_0 = \cosh(k), \quad e_0 = e^{-k}.$$

After straightforward algebra the characteristic equation for σ follows from (26) to (29):

$$\sigma^3 + a_2(k)\sigma^2 + a_1(k)\sigma + a_0(k) = 0, \tag{31}$$

where a_2, a_1, and a_0 are real functions of the dimensionless wavenumber k given by

$$a_2 = b_0 + b_1 + b_2 + b_5 - b_3 - b_4,$$
$$a_1 = (b_1 + b_5)(b_2 - b_3) + b_1 b_5 + b_0(b_2 + b_3 + b_6) - b_4(b_1 + b_6) - b_0 b_7, \tag{32}$$
$$a_0 = (b_2 - b_3)b_1 b_5 + b_0 b_6(b_2 + b_3) - b_4 b_1 b_6 - b_0 b_7 b_5,$$

where

$$b_0 = f_f s_1^2, \quad b_1 = -f_f s_1 c_1, \quad b_2 = -k,$$
$$b_3 = -(f_f - f_b)c_2 s_2, \quad b_4 = (f_f - f_b)s_2 s_2^2, \tag{33}$$
$$b_5 = f_b s_0 e_0, \quad b_6 = f_b c_0 e_0, \quad b_7 = (f_b - f_f)c_2^2.$$

For a given k, (31) is a cubic polynomial with real coefficients and has therefore three roots that can be either all real or one real and two complex conjugated, $\sigma = \sigma_r \pm i\sigma_i$, where i is the imaginary unit and $\sigma_r > 0$ and $\sigma_i > 0$. The basic current is stable for the first case. For the second case the current is unstable, and the positive imaginary part of the complex root, σ_i, is the growth rate of the shear wave.

3.1. Analysis of the Frontshear and Backshear Instability Curves

To explain the behavior of the complex solutions of (31), in Figure 2 their imaginary and real parts are presented. Figure 2a shows the instability curves (σ_i versus k) calculated with $\delta_2 = 0.5$ for different values of δ_1. As could be expected, for $\delta_1 = 0$ the solution coincides with the BH solution and shows an interval of wave numbers $k_{b,mn} < k < k_{b,mx}$ (for the example $k_{b,mn} = 1.38$ and $k_{b,mx} = 3.42$) for which the shear waves are unstable with a maximum growth rate $\sigma_{i,b} = 0.33$ achieved at $k_b = 2.5$.

For small values of δ_1 the solution shows two ranges of unstable wave numbers. One of the instability curves has almost the same shape and magnitude as the one obtained by BH, and since it responds to backshear changes, it will be referred to as the backshear instability curve. The additional

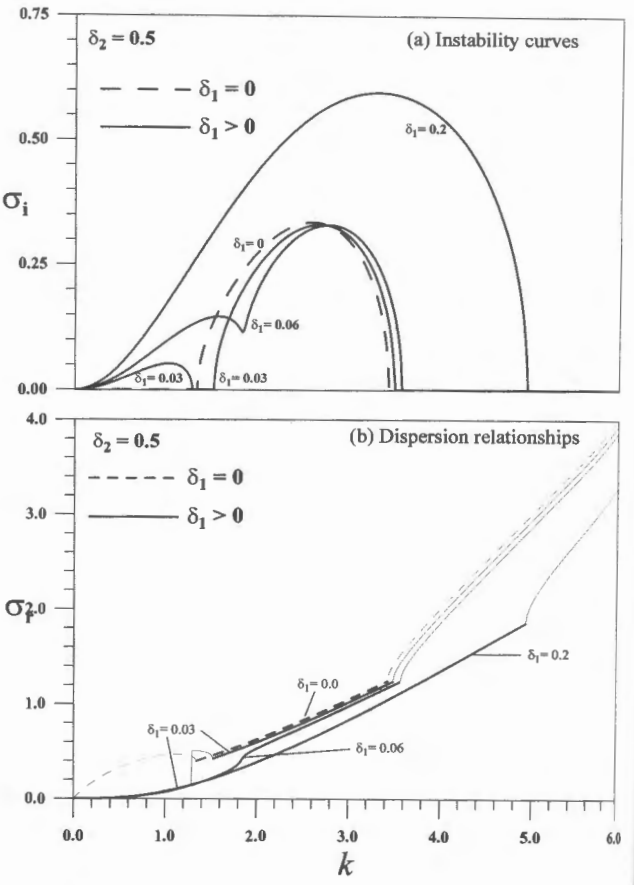

Figure 2. Complex solutions of the dispersion equation: (a) positive imaginary part of σ and (b) real part of σ calculated for $\delta_2 = 0.5$ and different values of δ_1.

range $k_{f,mn} < k < k_{f,mx}$ of unstable wave numbers is clearly associated with the existence of the frontshear f_f since their growth rates increase with f_f. This curve is referred to as the frontshear instability curve. As an example, for $\delta_1 = 0.03$ this interval is $0 < k < 1.27$ and has a maximum growth rate of $\sigma_{i,f} = 0.05$, smaller than $\sigma_{i,b}$, at $k_f = 1.06$. For $\delta_1 = 0.06$ both curves intersect, showing two relative maxima; again, the one corresponding to the backshear remains almost unchanged. For $\delta_1 = 0.2$ there is just one unstable curve with a fastest growth rate $\sigma_i = 0.59$ at $k = 3.3$, significantly greater than previous values of $\sigma_{i,b}$; moreover, the range of unstable wave numbers is wider, extending from $k_{mn} = 0$ to $k_{mx} = 4.92$. Notice that k_{mn} is asymptotically zero, which means that when a shear exists at the frontshear region, the range of wavelengths for which the shear waves are unstable is not bounded.

In Figure 2b the values of σ_r of the unstable modes are highlighted with a thicker curve line. Both the front and back shear instability curves have almost linear dispersion relationships with the same slope.

Figure 3 shows the maximum growth rate σ_i in terms of f_f for the values $\delta_2 = 0.2$, $\delta_2 = 0.5$, and $\delta_2 = 0.7$, which represent three different backslopes. For each backslope $f_b(\delta_2)$ there is a critical value of the frontshear $f_f^{c1}(\delta_2)$ (or equivalently, a critical value $\delta_1^{c1}(\delta_2)$) such that for $f_f < f_f^{c1}$ the curve has two branches corresponding to the two relative maxima of the instability curves, one due to the frontshear and the other due

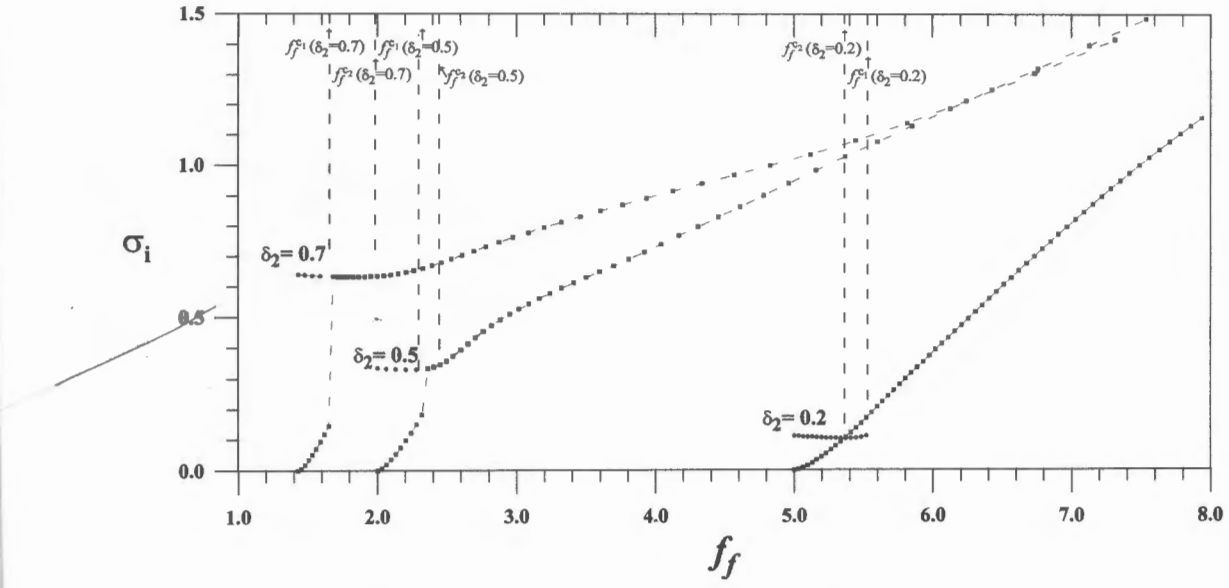

Figure 3. Maximum growth rates in terms of f_f for different values of δ_2.

to the backshear. For $f_f > f_f^{c1}$, since the (k, σ_i) curve has one maximum, there is just one branch. For $f_f < f_f^{c1}$ the frontshear branch $\sigma_{i,f}(f_f)$ increases with f_f starting at $\sigma_i = 0$, whereas the backshear branch is nearly horizontal, revealing that the existence of the frontshear does not affect the backshear instability.

The behavior of the only branch existing for $f_f > f_f^{c1}$ depends, however, on the relative intensity of the frontshear and backshear. This branch starts at the level of the maximum of both growth rates at f_f^{c1}, which for steep (δ_2 large) backslopes corresponds to the backshear fastest growing mode (see curves obtained for $\delta_2 = 0.5$ and 0.7), whereas for mild (δ_2 small) backslopes is achieved by the frontshear mode (see curve for $\delta_2 = 0.2$).

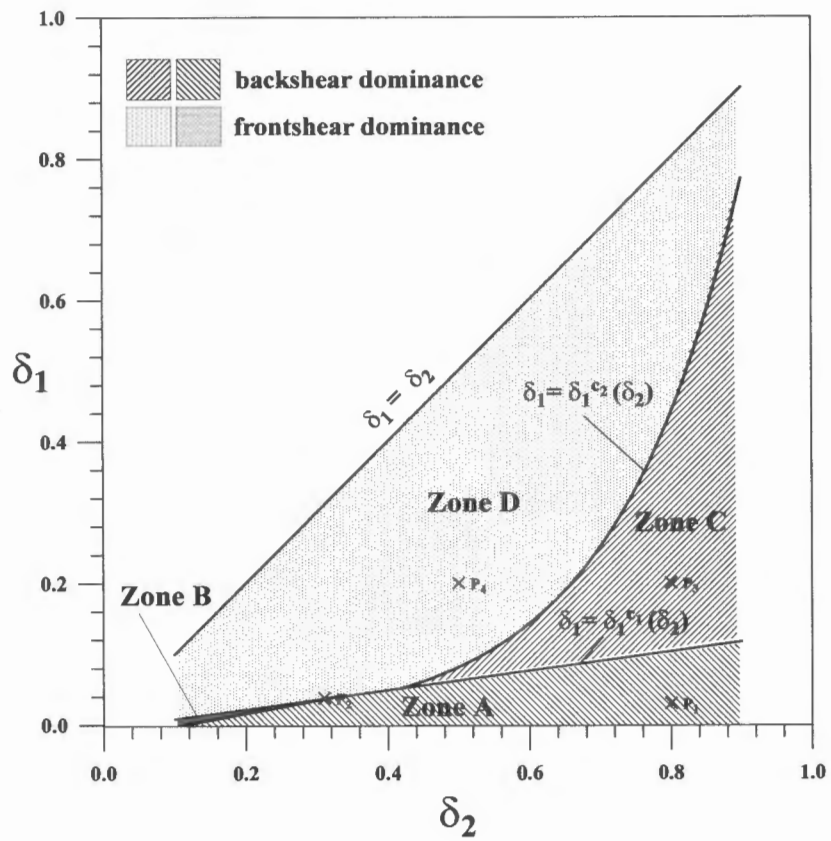

Figure 4. Division of the domain (δ_2, δ_1) into zones attending to frontshear or backshear wave dominance.

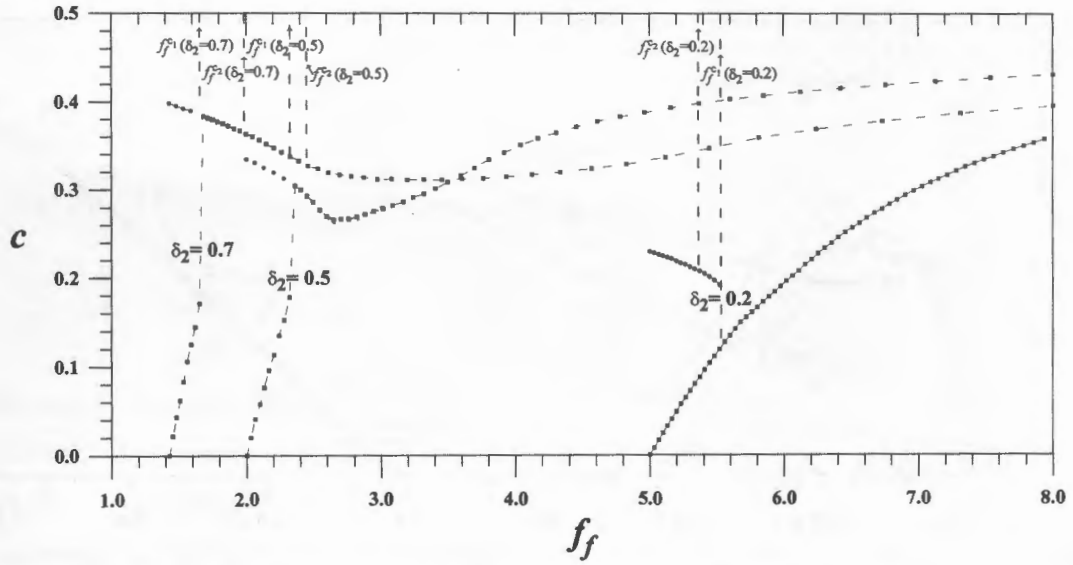

Figure 5a. Dimensionless celerities in terms of f_f for different values of δ_2.

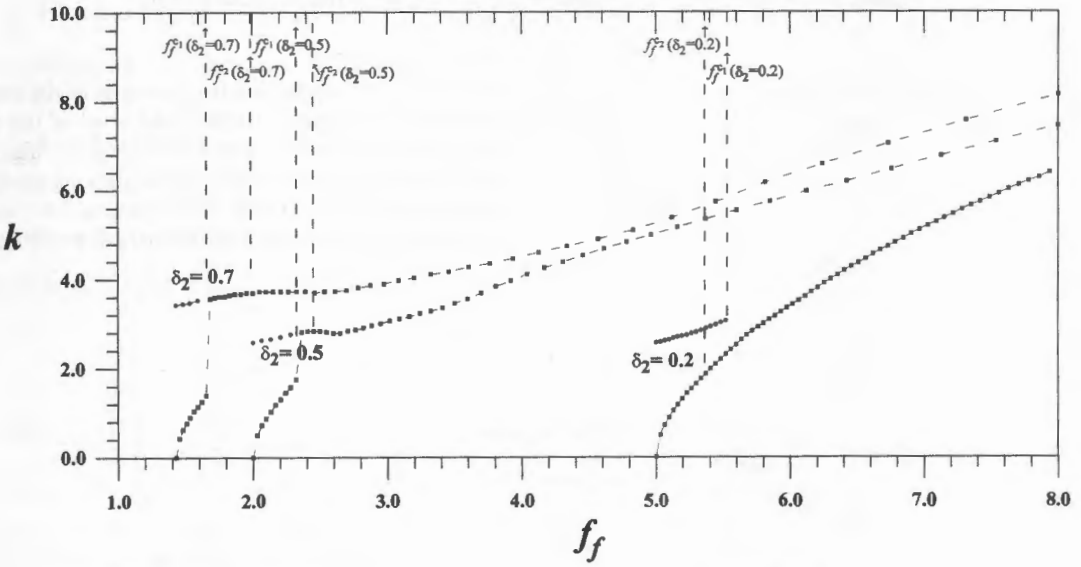

Figure 5b. Dimensionless wave numbers in terms of f_f for different values of δ_2.

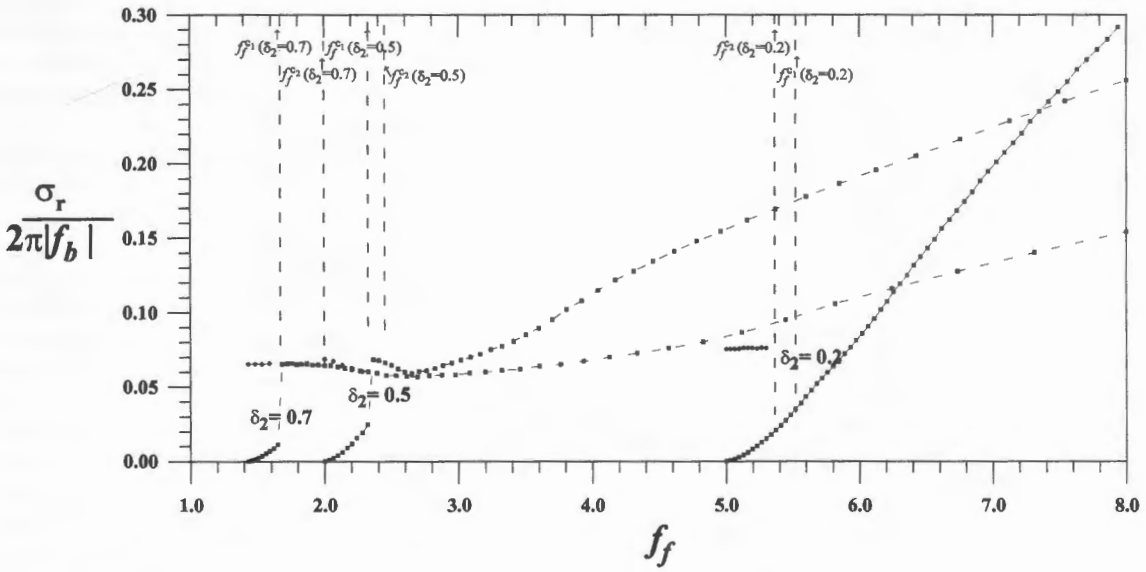

Figure 5c. Dimensionless wave frequencies relative to $|f_b|$ in terms of f_f for different values of δ_2.

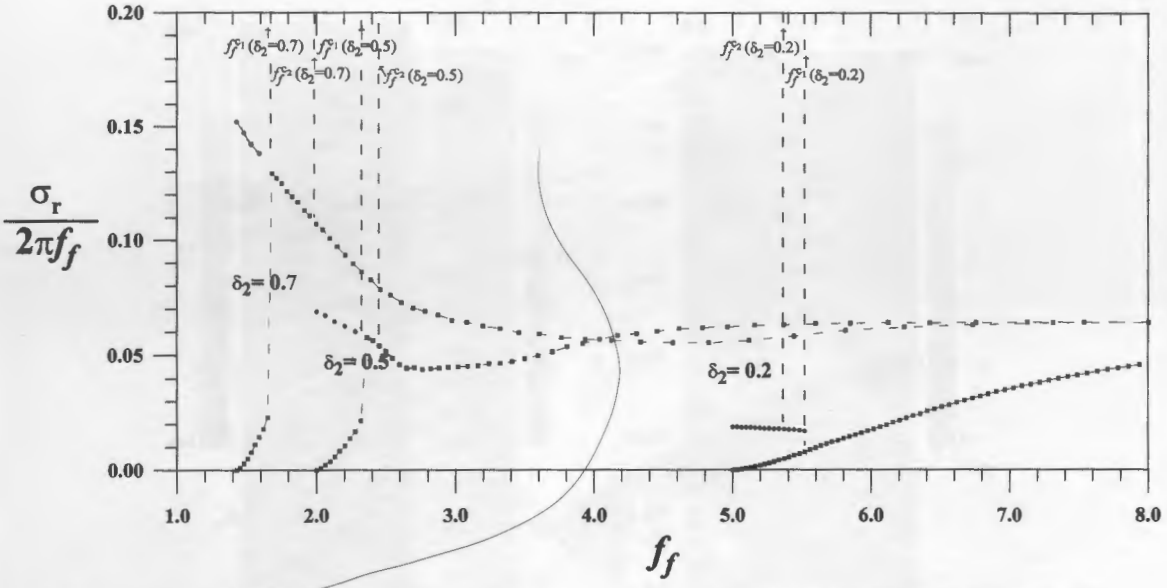

Figure 5d. Dimensionless wave frequencies relative to f_f in terms of f_f for different values of δ_2.

For $f_f > f_f^{c1}$ and steep (δ_2 large) backslopes there is a range of values for which the backshear instability is dominant since the growth rate is insensitive to the increase of f_f. This pattern is followed up to a second critical value $f_f^{c2}(\delta_2)$ (or equivalently, a critical value $\delta_1^{c2}(\delta_2)$) for which the growth rate starts to increase with f_f. Here f_f^{c2} establishes the transition from backshear to frontshear predominance for values of $f_f > f_f^{c2}$.

On the contrary, for small values of δ_2 that represent mild

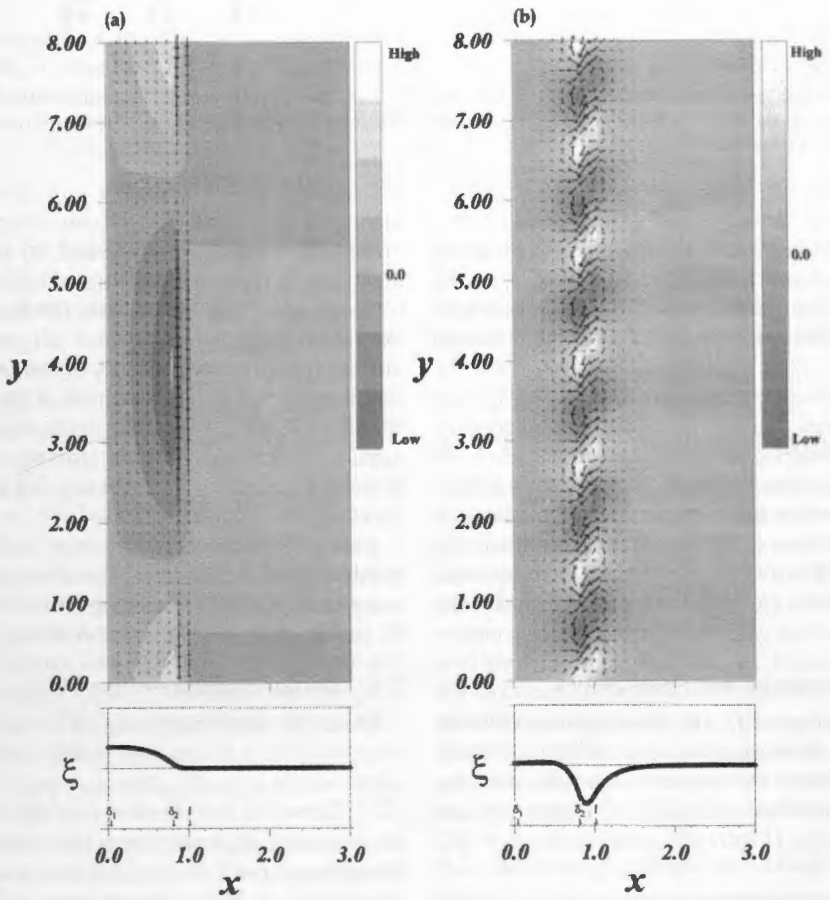

Figure 6. Snapshot of the flow structure, the stream function, and the free surface elevation of the (a) frontshear wave and (b) backshear wave obtained for $P_1(\delta_2 = 0.8, \delta_1 = 0.03)$.

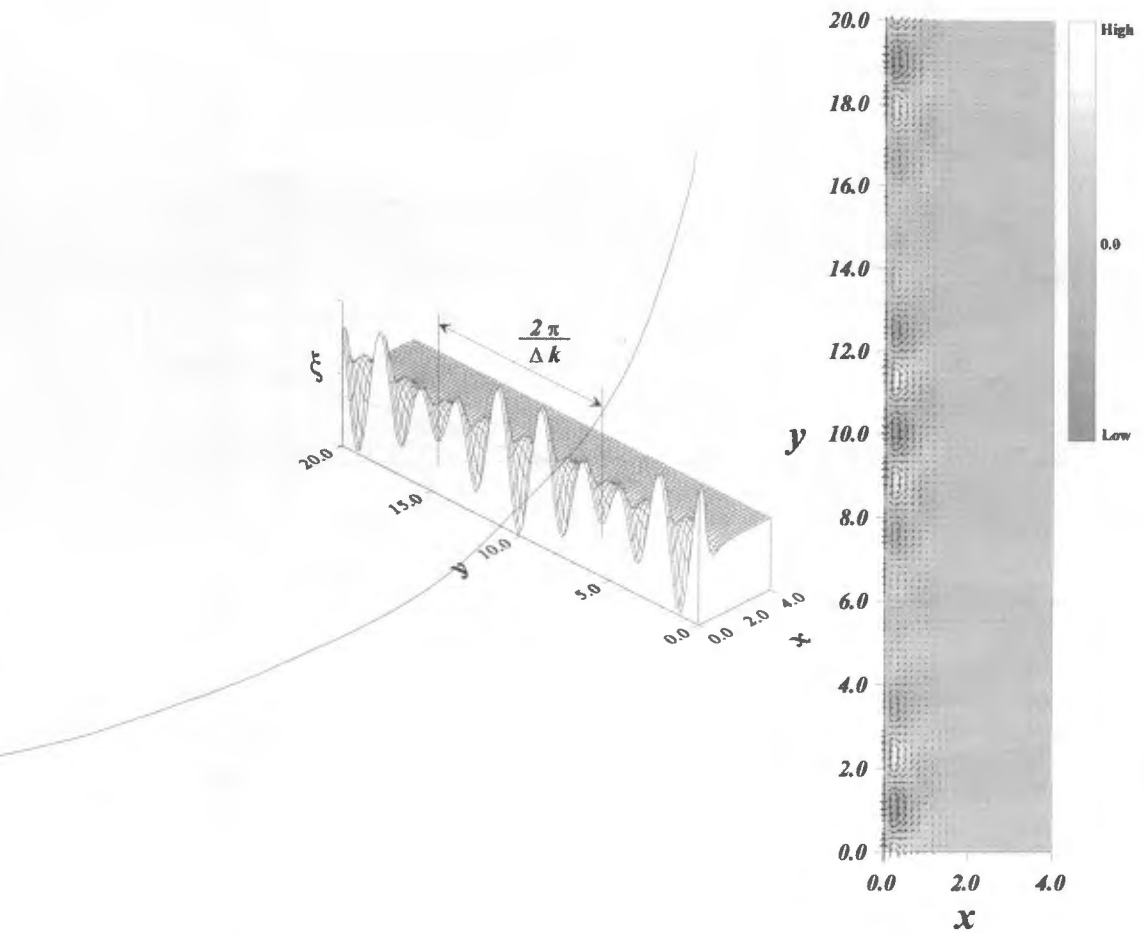

Figure 7. Snapshot of the flow structure, the stream function, and the three-dimensional free surface elevation of the shear wave resulting from the superposition of the backshear and frontshear waves obtained for $P_2(\delta_2 = 0.31, \delta_1 = 0.038)$.

backslopes the frontshear instability is dominant at the branching point f_f^{c1}, having crossed at a critical value $f_f^{c2}(f_b) < f_f^{c1}$ the backshear branch. For $f_f > f_f^{c1}$ the growth rate increases with increasing f_f following the tendency of the frontshear branch obtained for values $f_f < f_f^{c1}$.

Attending to this behavior, the domain of values (δ_2, δ_1) may be divided into four zones that will be referred to as zone A, zone B, zone C, and zone D, delimited by the curves $\delta_1 = \delta_1^{c1}(\delta_2)$ and $\delta_1 = \delta_1^{c2}(\delta_2)$ (see Figure 4). In zones A and B the instability curves have two relative maxima; the backshear is dominant in zone A, whereas the frontshear is dominant in zone B. In zones C and D there is only one relative maximum of the growth rate related to the backshear in zone C and to the frontshear in zone D.

3.2. Characteristic Timescales and Space Scales

Figure 5 shows, in terms of f_f, the dimensionless velocity phase c (Figure 5a), the dimensionless wave number k (Figure 5b), and the dimensionless wave frequency normalized by the absolute value of the backshear, $\sigma_r/(2\pi|f_b|)$ (Figure 5c), and by the frontshear, $\sigma_r/(2\pi f_f)$ (Figure 5d), obtained for $\delta_2 = 0.2$, 0.5, and 0.7.

The BH estimate of the shear wave celerity, $c \simeq V_0/3$, is still valid no matter whether the instability comes from the frontshear or the backshear. There is an exception: the very long frontshear waves (zones A and B) may have phase speeds significantly smaller increasing with f_f linearly up to $c \simeq V_0/5$.

Moreover, in agreement with BH model the frequency of the backshear mode is proportional to f_b, $\sigma_r/(2\pi|f_b|) \simeq 0.07$. On the other hand, the frequency of the frontshear mode tends to be proportional to f_f, also with $\sigma_r/(2\pi f_f) \simeq 0.07$, for $\delta_2 = 0.7$ and $\delta_2 = 0.5$; for $\delta_2 = 0.2$ a similar trend is observed but with smaller frequencies. Again, for the long frontshear waves (zones A and B) the frequency can be significantly smaller, $\sigma_r/(2\pi f_f) \simeq 0.01$.

Finally, the wave number of the backshear mode follows the predictions of BH, $k \simeq \pi$. The wave number of the frontshear wave increases with f_f ranging from $k \simeq \pi$ to $k \simeq 2\pi$ in zone D and up to $k \simeq 2$ in zones A and B.

3.3. Spatial Structure of the Flow

Once the wave frequency of an unstable shear wave with wave number k is obtained, fixing the value of A_0, the coefficients A_1, B_1, A_2, B_2, and A_3 can be determined from (26)-(29). The water surface elevation will then be given by (20). In the following, the spatial structure of the shear waves obtained for different pairs of (δ_2, δ_1) will be analyzed. Their values are represented in Figure 4 and denoted by P_1, P_2, P_3, and P_4.

Figure 6 shows a snapshot of the velocity field of (a) the front shear and (b) the backshear waves with relative fastest

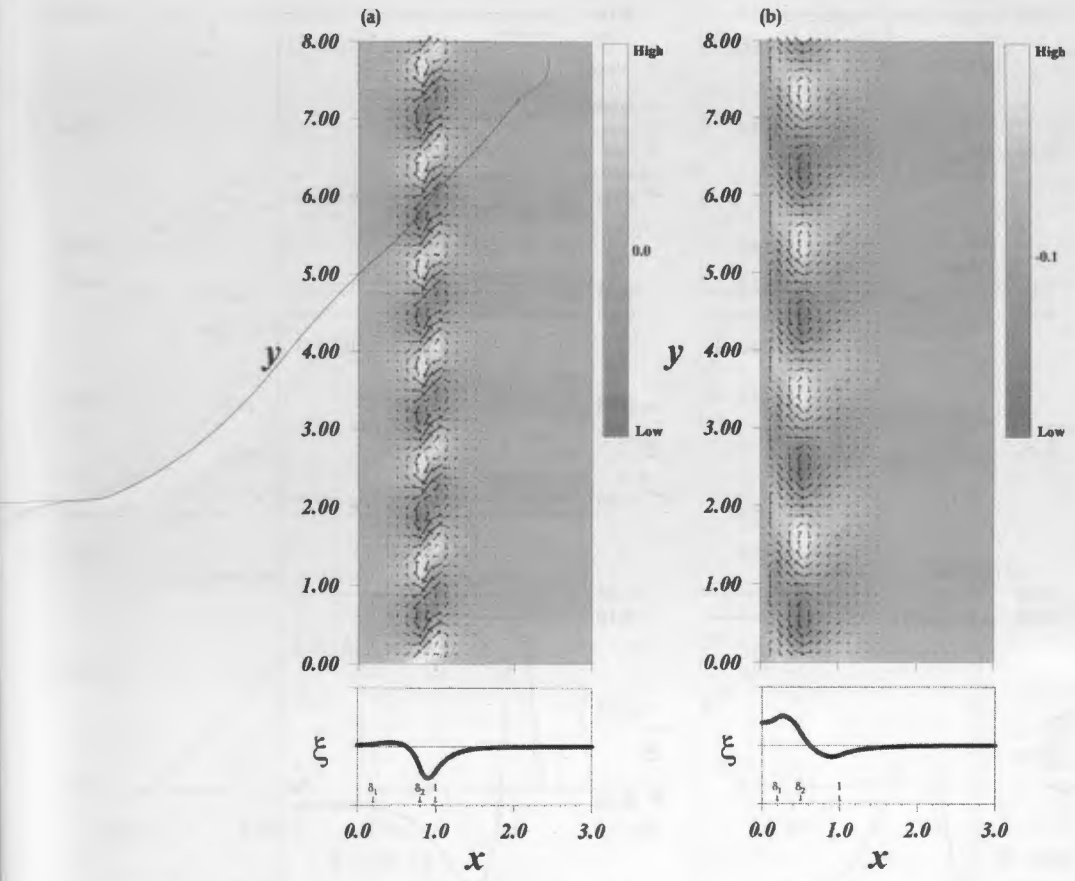

Figure 8. Snapshot of the flow structure, the stream function, and the free surface elevation of the (a) backshear wave obtained for $P_3(\delta_2 = 0.8, \delta_1 = 0.2)$ and (b) frontshear wave obtained for $P_4(\delta_2 = 0.5, \delta_1 = 0.2)$.

growth rates, calculated for $\delta_2 = 0.8$ and $\delta_1 = 0.03$ (denoted by P_1), where the backshear is dominant (zone A). Underneath the arrows the isolines of the stream function have been drawn. Figure 6 also includes the corresponding free surface elevation as a function of x. The front shear wave, with a wavelength $\lambda_f = 9.62$, extends from the shoreline over the width of the current. The backshear wave, with a wavelength $\lambda_f = 1.32$, extends over a wider zone of about one and a half the width of the current, and the significant part of the flow due to the backshear is confined to the region $0.5 \leq x \leq 1.5$.

For mild (δ_2 small) backslopes there is a given front slope for which the frontshear and the backshear waves have approximately the same growth rate σ_i, leading to the possibility of having both instabilities at the same time, which are two propagating waves that have close angular wave frequencies $\sigma_{r,f}$ and $\sigma_{r,b} = \sigma_{r,f} + \Delta\sigma_r$ and close wave numbers k_f and $k_b = k_f + \Delta k$. If the water surface elevation of the frontshear and the backshear waves are $\xi_f(x, y, t) = \Re\{\hat{\xi}_f(x) \exp[i(k_f y - \sigma_{r,f}t)]\}$ and $\xi_b(x, y, t) = \Re\{\hat{\xi}_b(x) \exp[i(k_b y - \sigma_{r,b}t)]\}$, respectively, the resulting wave is then

$$\xi(x, y, t) = \Re\{[\hat{\xi}_f(x) + \hat{\xi}_b(x)e^{i(\Delta k y - \Delta\sigma_r t)}]e^{i(k_f y - \sigma_{r,f}t)}\}, \quad (34)$$

where $\xi(x, y, t)$ is a wave whose amplitude is modulated in the longitudinal direction with wavelength $\lambda = 2\pi/\Delta k$ and travels in the y direction with celerity $c = \Delta\sigma_r/\Delta k$ (see Figure 7 calculated for $\delta_1 = 0.038$ and $\delta_2 = 0.31$ (denoted by P_2 in Figure 4)).

The case analyzed in zone C has the same backshear as the case in zone A, but the frontshear has a larger value. In both cases the backshear is dominant, and the wave field pattern is similar (see Figure 8a obtained for $\delta_1 = 0.2$ and $\delta_2 = 0.8$; P_3 in Figure 4). Finally, in zone D the frontshear wave has a smaller wavelength than the one obtained in zone A and extends over a wider zone.

4. Numerical Analysis of Realistic Profiles

The model presented above explains the basic mechanism of instabilities due to an extremum of the background vorticity at the front side of the velocity profile. For a more realistic description the analysis of smooth current profiles in a beach of variable depth has been done by solving (15), (16), and (17) numerically, which takes into account bottom friction and lateral momentum diffusion [see *Falqués and Iranzo*, 1994]. A series of current profiles with and without background vorticity extremum at the front over a plane sloping beach are analyzed. Then, instability analysis is performed on a current profile obtained from data measured at Leadbetter Beach, and results are compared with field observations.

4.1. Instability Analysis on a Plane Sloping Beach

A series of three longshore currents in a plane beach of slope 1:15, with the same profile seaward of the location of maximum velocity and varying frontshear values, is analyzed.

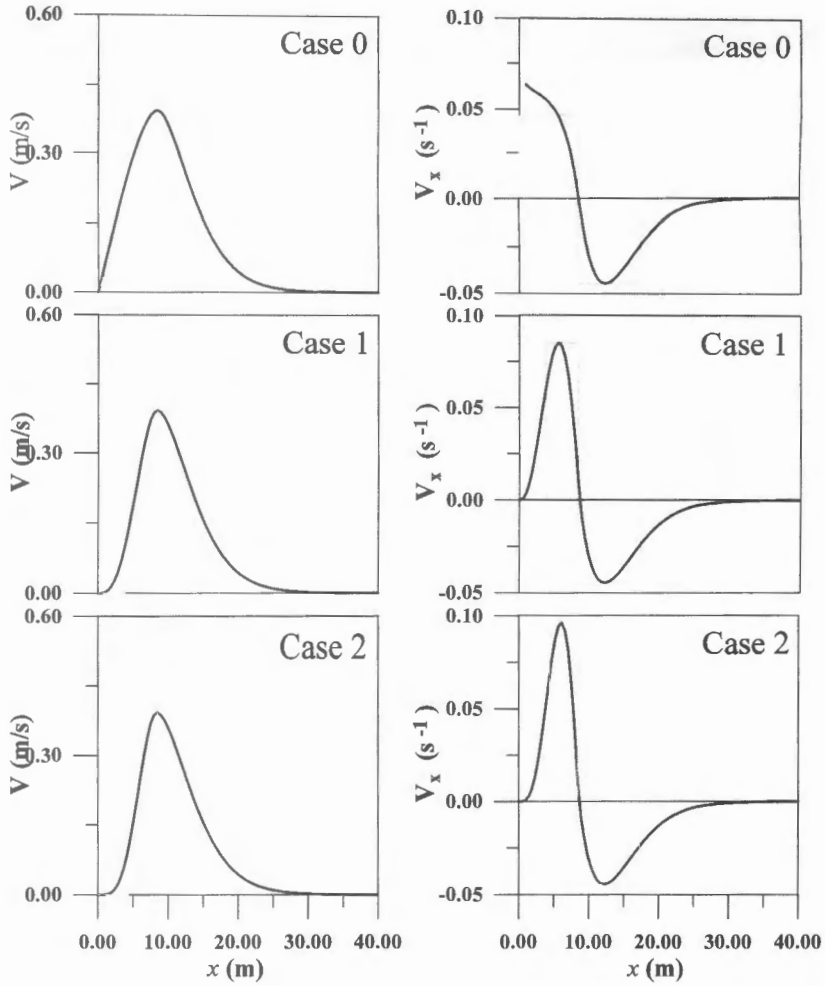

Figure 9. Current profiles and velocity gradients of cases 0, 1, and 2.

This moderate reflective profile was chosen expecting an instability behavior comparable to the extended BH model. In all cases the shear extremum at the back is $V_{x,b} = -0.044\ s^{-1}$. Case 0 corresponds to a profile without frontshear extremum, and cases 1 and 2 have a frontshear extremum with values of $V_{x,f} = 0.085\ s^{-1}$ and $V_{x,f} = 0.096\ s^{-1}$, respectively. Figure 9 shows the three velocity profiles and their respective background vorticities together with the simplified curves for the analysis with the extended BH model.

Figure 10 shows the instability curves obtained for the three cases by neglecting the damping effect of bottom friction and turbulent diffusion (Figure 10a) and with a drag coefficient $c_d = 0.0001$ and a kinematic eddy viscosity $(\nu_t)_{max} = 0.01\ m^2\ s^{-1}$ (Figure 10b). For the same cases, Figures 11a and 11b show the corresponding dispersion relationships.

Case 0 presents an instability diagram with a single (nonspurious) mode with maximum growth rate achieved at $k = 0.089\ m^{-1}$. Cases 1 and 2 present two unstable curves. The fastest growing mode of the first one is placed at $k \sim 0.078\ m^{-1}$ for both cases, and the one of the second curve is placed at $k = 0.156\ m^{-1}$ for case 1 and at $k = 0.201\ m^{-1}$ for case 2. Similar curves are obtained with and without damping, and the only significant effect of the viscosity and bottom friction is to reduce the growth rates of all modes.

The first modes of cases 1 and 2 resemble the single mode of case 0, and they are insensitive to the change of the frontshear value. Their celerities are $c \sim 0.3\ m\ s^{-1} = 3V_{max}/4$, where V_{max} is the maximum value of the current, and their wave numbers are in the range $2\pi/3 < kl < 2\pi/1.5$, where $l \sim 25$ m is the width of the current. All these values are in the ranges expected for a vorticity wave due to the extremum of the background vorticity at the backside of the profile. Moreover, the analysis of similar profiles, not presented here for simplicity, have shown that the growth rate increases with f_b.

The second unstable curve exists only for the profiles with a shear at the front. They have similar wave numbers, $k \sim 0.18\ m^{-1}$, and their celerities are $\sim c \sim 0.1\ m\ s^{-1}$. The highest growing rate corresponds to the case of the largest front shear.

These results suggest that the first modes of cases 1 and 2 are associated with the extremum of the background vorticity at the back, whereas the second modes are due to the one at the front. Because of the dependence of the background vorticity on the beach profile, numerical results give a frontshear wave with a larger wave number than the backshear wave. By applying the analytical model, for the case of two unstable curves, the front shear fastest growing mode has a smaller wave number than the corresponding backshear wave. This behavior is due to the differences in shapes of the beach profiles used: a flat sloping bottom was tested for the numerical simulations and a constant water depth for the simplified model. Numerical simulations of the velocity currents of cases 1 and 2 with a constant water depth beach profile predicted, as expected,

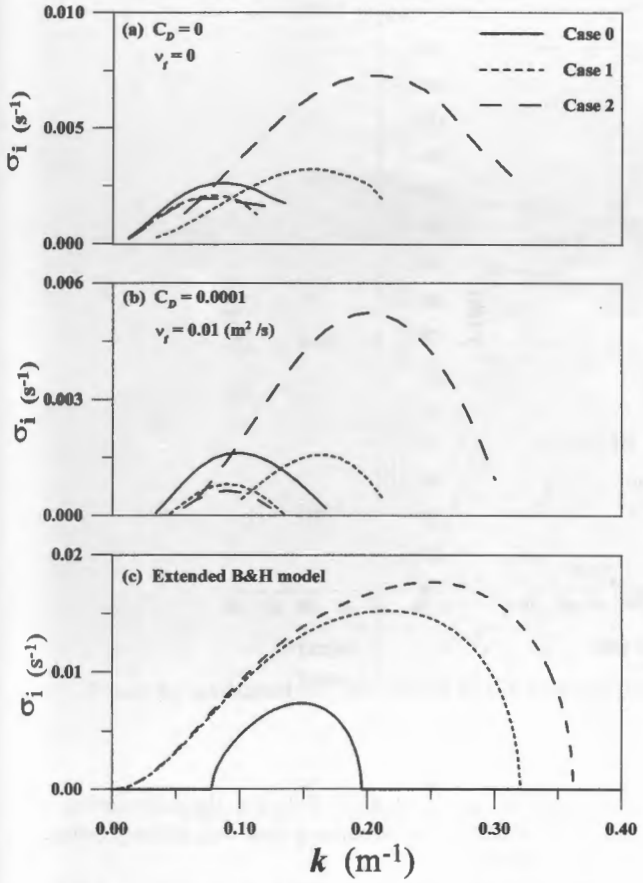

Figure 10. Instability curves obtained for cases 0, 1, and 2.

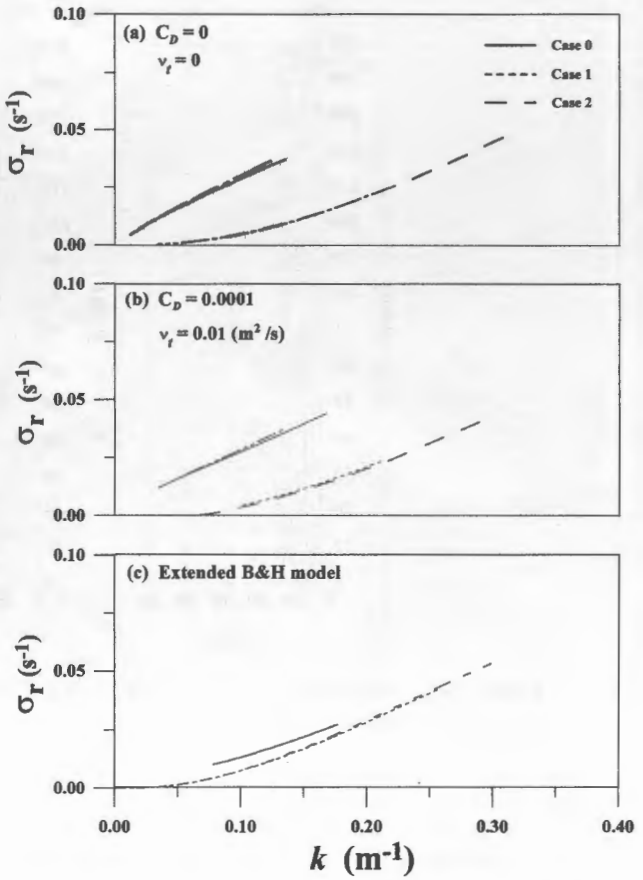

Figure 11. Dispersion relationship curves obtained for cases 0, 1, and 2.

instability and dispersion curves almost identical to the ones obtained with the analytical model.

In order to compare cases 1 and 2 with the extended BH model, simplified current profiles with the same shears at the front and at the back sides were analyzed. The parameters used were $V_0 = 0.39$ m s^{-1}, $x_0 = 17.28$ m, $\delta_2 = 0.48$, and $\delta_1 = 0.22$ for case 1 and $\delta_1 = 0.25$ for case 2, whose corresponding nondimensional shears are $f_b = -1.92$, $f_{f_1} = 3.84$, and $f_{f_2} = 4.34$ (see Figure 9c). The extended BH model anticipates frontshear dominance in both cases with growing rates, $\sigma_{i1} = 0.015$ s^{-1} and $\sigma_{i2} = 0.017$ s^{-1} (see Figure 10c), which are about twice the values obtained with the numerical model. This may be due to the modelization of the shears in the simplified current profile, to the sloping sea bed, and to the free surface effects [*Falqués and Iranzo*, 1994]. However, the values of the wave numbers ($k_1 = 0.215$ m^{-1} and $k_2 = 0.249$ m^{-1}) and celerities ($c_1 = 0.12$ m s^{-1} and $c_2 = 0.14$ m s^{-1}) are in good agreement with the numerical results.

Figure 12 shows the flow structure of (a) the backshear wave of case 0, (b) the backshear wave of case 1, and (c) the front shear wave of case 1. For the velocity profile without a shear extremum at the front the back vorticity wave extends from the shoreline in a zone of width approximately twice the width of the longitudinal current.

The significant part of the front shear wave of case 1 is restricted to a narrow region of width $l_1 \sim 9$ m, delimited approximately by the shoreline and the line of the maximum current velocity, $x = x_m$. Its celerity is roughly $c \sim 0.5\bar{V}$, where $\bar{V} \sim 0.15$ m s^{-1} is the average velocity in that region, suggesting that the frontshear wave is convected by the longitudinal current between $x = 0$ and $x = x_m$. The presence of the front shear reduces the flow field associated with the backshear wave between the shoreline and the location of maximum current velocity.

4.2. Comparison With Field Data

Theoretical results are compared with field data measured during the 1980 Nearshore Sediment Transport Studies experiment at Leadbetter Beach, Santa Barbara, California. For the analysis the velocity profile fitted by *Dodd et al.* [1992] to data measured on February 4 (run c) with the model by *Thornton and Guza* [1986] was chosen as a base. This profile, hereinafter referred to as case LB_0, has a single inflexion point located in the zone seaward of the location of maximum velocity, with a value of $V_{x,b} = -0.024$ s^{-1}.

Run c is the third in a series of three runs measured in an ~4 hour interval that were analyzed by *Dodd et al.* [1992]. To account for variations in tidal elevation and waves over that interval, they fitted three velocity profiles to longshore current measurements, obtaining very similar profiles.

In order to compare the situation analyzed by *Dodd et al.* [1992] with results for a current profile with an additional shear at the front, a velocity current that conserves the shape of the profile of case LB_0 seaward of the location of maximum velocity was adopted. In the shoreward part of the current a cubic spline was fitted to the bin-averaged data from the three consecutive runs. The resulting velocity profile, which will be re-

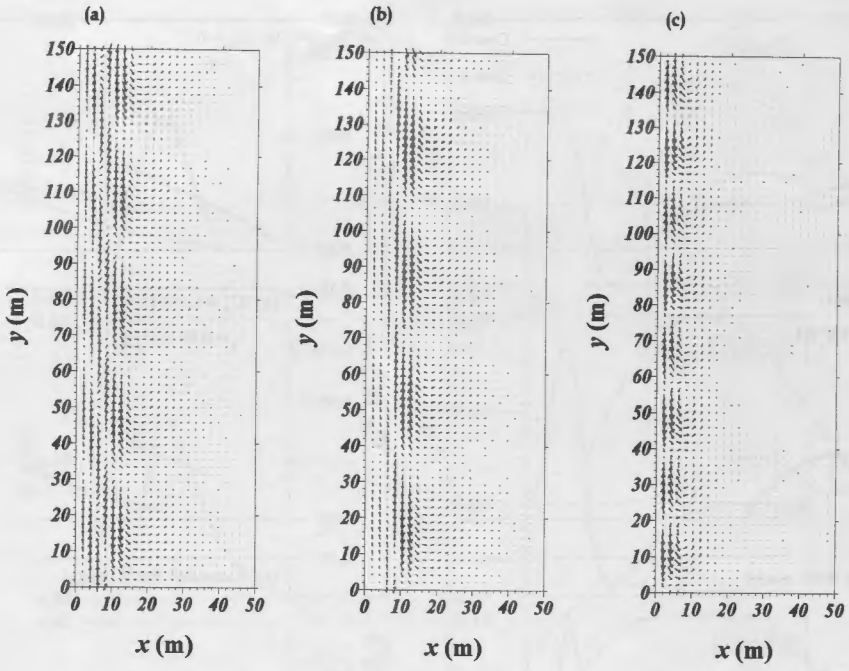

Figure 12. Snapshot of the flow structure of (a) the backshear wave of case 0, (b) the backshear of case 1, and (c) the frontshear wave of case 1.

ferred to as case LB_1, has a value of the shear extremum at the front: $V_{x,f} = 0.033\ s^{-1}$ (see Figure 13).

For the instability analysis, in order to be consistent with the analysis performed by *Dodd et al.* [1992], diffusion terms were neglected and the same law for the bottom shear stress was adopted. Different values of the bottom friction coefficient in the range $0 \leq c_d \leq 0.009$ were tested. Case LB_0 presents an unstable mode with a fastest growing mode at $k \simeq 0.055\ m^{-1}$ for values up to $c_d = 0.007$ (Figure 14), a value smaller than that used by *Dodd et al.* [1992] for the calculation of the velocity profile, an inconsistency that was already pointed out by the authors.

The instability frequency-cyclic wave number relationship (Figure 15) agrees with *Dodd et al.*'s [1992] predictions and falls in the same region as the variance computed from field observations. The instability curves obtained for case LB_1, with fastest growing modes located at $k \sim 0.065\ m^{-1}$, a slightly higher value of k, have larger growth rates and almost

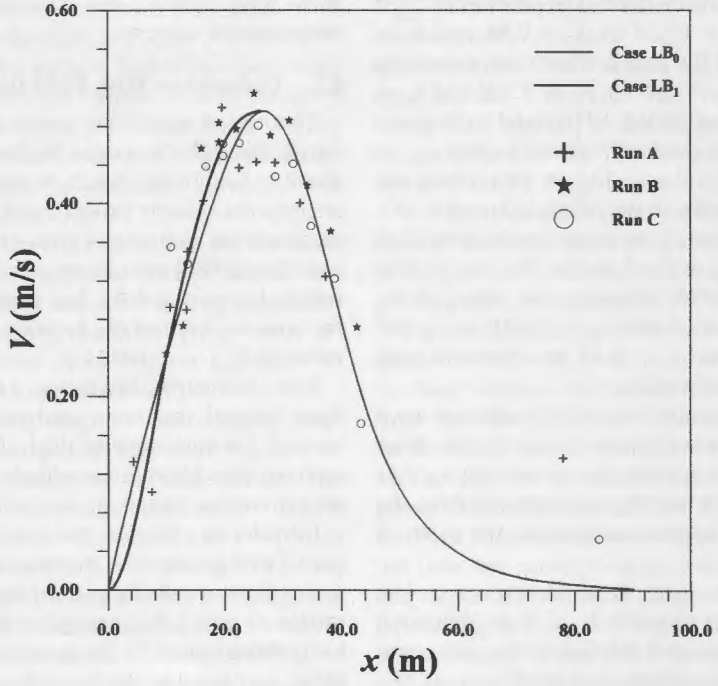

Figure 13. Velocity profiles of cases LB_0 and LB_1 and data measured at Leadbetter beach on February 4.

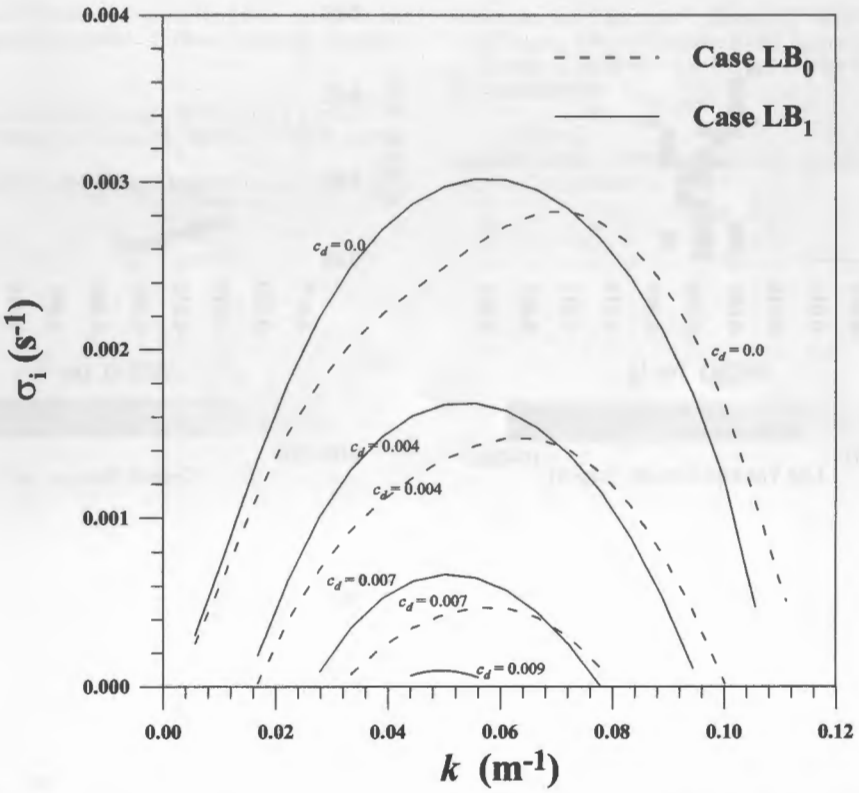

Figure 14. Unstable modes obtained for cases LB_0 and LB_1 for different values of c_d.

identical dispersion relationships than those obtained for case LB_0. Moreover, the unstable modes exist for values of c_d up to 0.009, a value that is the same as that used by *Dodd et al.* [1992] for the calculation of the velocity profile.

Figure 15 shows (a) the $f - k$ values measured at Leadbetter on February 4 and the values predicted for (b) case LB_0 with $c_d = 0.004$, (c) case LB_1 with $c_d = 0.004$, and (d) case LB_1 with $c_d = 0.009$. Predicted and measured values agree fairly well.

5. Conclusions

An analytical study and a numerical model [see *Falqués and Iranzo*, 1994] are used to analyze the instabilities of a longshore current whose background vorticity shows two extrema at both sides of the location of the maximum velocity. The analytical model is based on an idealized triangular velocity profile inspired on BH and defined in terms of two parameters, δ_1 and δ_2, that determine the intensity of the frontshear and the backshear. A cubic polynomial is obtained as a dispersion relationship, which is solved to obtain the growth rate, the frequency, and the flow pattern of the unstable modes. Because of the limitation imposed by the cubic dispersion relation, only one unstable mode is obtained for each wave number. However, looking at the response of the solution to the backshear and to the frontshear and looking at the shoreward or seaward location of the flow pattern, a backshear wave (BS) or a frontshear wave (FS) can be identified. The dominance of the backshear or the frontshear is discussed in terms of δ_1 and δ_2; four regions can be distinguished (see Figure 4). In zones A and B the instability curves (growth rate against wave number) show two relative maxima, one can be associated with the BS and another with the FS; in zone A the BS peak is dominant, whereas the FS peak is dominant in zone B. For values of (δ_2, δ_1) in zones C and D the instability curves show only one maximum that can be associated either to the backshear (zone C) or to the frontshear (zone D). In zone B it is possible to find values of (δ_2, δ_1) for which the instabilities associated with the frontshear and the backshear have similar growth rates, with close wave frequencies and wave numbers, leading to the possibility of having a shear wave modulated in the alongshore direction.

For realistic current profiles in a beach of variable depth the numerical analysis confirms the existence of instabilities associated with the frontshear. The frontshear waves extend over the width of the current, and their amplitude is significant only in a region bounded by the shoreline and the location of the maximum current with a characteristic celerity that suggests that the frontshear wave is convected by the portion of the longitudinal current in that region. The presence of the frontshear wave reduces the amplitude of the backshear wave between the shoreline and the location of maximum velocity.

Furthermore, stability analysis was performed numerically on both (1) a profile analyzed by *Dodd et al.* [1992] with only one extremum of background vorticity and (2) a profile obtained from data measured at Leadbetter Beach that is slightly different at the shoreward region, having an additional extremum of background vorticity. The second profile has a frontshear instability mode that is more unstable than the dominant mode of the first one. In fact, this frontshear mode is still slightly unstable for a bottom shear stress with a drag coefficient of $c_d = 0.009$, i.e., the value chosen by *Dodd et al.* [1992] to achieve a good agreement between the measured and the predicted intensity of the current. Then, the fact that the first

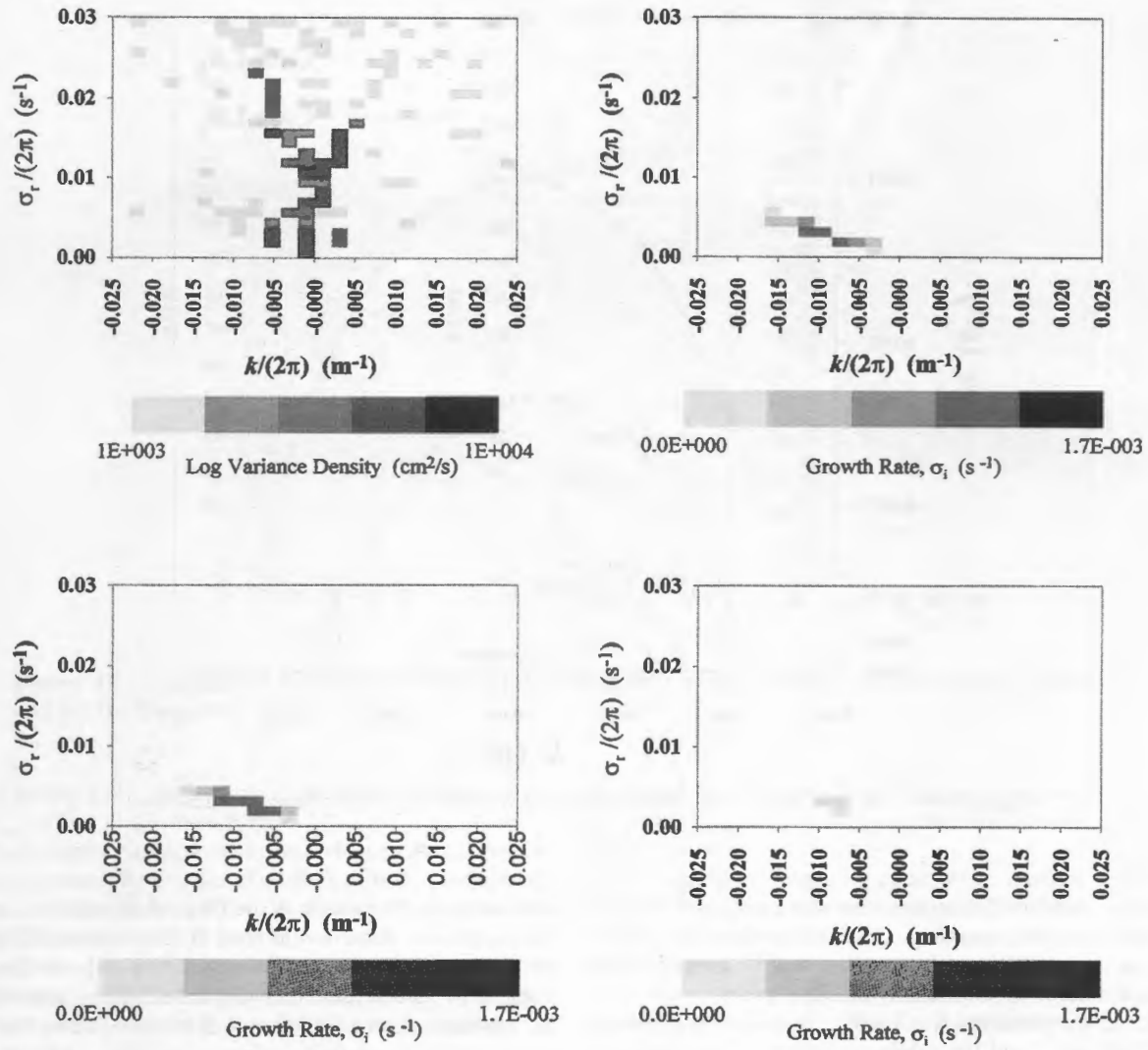

Figure 15. Comparison of measured and predicted frequency-cyclic wave number spectra: (a) iterative maximum likelihood estimator estimated frequency-cyclic wave number spectra at Leadbetter Beach on February 4, run c; (b) predicted frequency-cyclic wave number spectra for case LB_0, $c_d = 0.004$; (c) predicted frequency-cyclic wave number spectra for case LB_1, $c_d = 0.004$; and (d) predicted frequency-cyclic wave number spectra for case LB_1, $c_d = 0.009$.

profile is already stable for $c_d = 0.007$ leads to the conjecture that the instabilities observed at the Leadbetter experiment could be due to the frontshear instability.

Acknowledgments. A. Baquerizo was funded by a Marie Curie Fellowship of the European Community programme Improving Human Research Potential and the Socio-Economic Knowledge under contract HPMF-CT-1999-00229. M. Caballeria, M. A. Losada, and A. Falqués are indebted to the Commission of the European Communities in the framework of the Marine Science and Technology Programme (MAST) under contract MAS3970081 (Sasme Project).

References

Allen, J. S., P. A. Newberger, and R. A. Holman, Nonlinear shear instabilities of alongshore currents on plane beaches, *J. Fluid Mech.*, *310*, 181–213, 1996.

Bowen, A., and R. Holman, Shear instabilities of the mean longshore current, 1, Theory, *J. Geophys. Res.*, *94*, 23–30, 1989.

Caballeria, M., A. Falqués, and V. Iranzo, Shear instability of the longshore current as a function of incoming wave parameters, *Coastal Dynamics '97: Conference Proceedings*, edited by E. B. Thornton, 446–455, Am. Soc. of Civ. Eng., Reston, Va., 1998.

Dodd, N., On the destabilization of a longshore current on a plane beach: Bottom shear stress, critical conditions, and onset of instability, *J. Geophys. Res.*, *99*, 811–824, 1994.

Dodd, N., and E. B. Thornton, Growth and energetics of shear waves in the nearshore, *J. Geophys. Res.*, *95*, 16,075–16,083, 1990.

Dodd, N., J. Oltman-Shay, and E. B. Thornton, Shear instabilities in the long-shore current: A comparison of observation and theory, *J. Phys. Oceanogr.*, *22*, 62–82, 1992.

Falqués, A., and V. Iranzo, Numerical simulation of vorticity waves in the nearshore, *J. Geophys. Res.*, *99*, 825–841, 1994.

Oltman-Shay, J., P. Howd, and W. Birkemeier, Shear instabilities of the mean longshore current, 2, Field observations, *J. Geophys. Res.*, *94*, 31–42, 1989.

Ozkan-Haller, H. T., J. T. Kirby, Nonlinear evolution of shear instabilities of the longshore current: A comparison of observations and computations, *J. Geophys. Res.*, *104*, 25,953–25,984, 1999.

Putrevu, U., and I. A. Svendsen, Shear instability of longshore currents: A numerical study, *J. Geophys. Res.*, *97*, 7283–7303, 1992.

Reniers, A. J. H., J. A. Battjes, A. Falqués, and D. A. Huntley, A laboratory study on the shear instability of longshore currents, *J. Geophys. Res.*, *102*, 8597–8609, 1997.

Thornton, E. B., and R. T. Guza, Surf zone longshore currents and random waves: Field data and models, *J. Phys. Oceanogr.*, *16*, 1165–1178, 1986.

A. Baquerizo and M. A. Losada, Grupo de Puertos y Costas, Universidad de Granada, Ramón y Cajal, 4. 18071 Granada, Spain. (abaqueri@ugr.es)

M. Caballeria, Departament de Física y Matemàtica Aplicades, Universitat de Vic Carrer de la Laura, 13. 08500 Vic, Spain.

A. Falqués, Departament de Física Aplicada, Universitat Politècnica de Catalunya Jordi Girona, 1-3, mòdul B4-B5, Campus Nord, 08034 Barcelona, Spain.

(Received June 1, 1999; revised June 22, 2000; accepted December 29, 2000.)